Journal of Materials Science: Materials in Electronics (2019) 30:1663–1669
https://doi.org/10.1007/s10854-018-0437-7

Structure and property of lead-free (K,Na)NbO_3–($Bi_{1/2}Na_{1/2}$)ZrO_3–$CaTiO_3$ piezoelectric ceramics

Nan Zhang[1] · Jiagang Wu[1]

Received: 28 September 2018 / Accepted: 22 November 2018 / Published online: 26 November 2018

Abstract
Simultaneous improvement of piezoelectricity and temperature stability is vital for developing high-performance KNN-based lead-free materials. Here, effects of $CaTiO_3$ on phase structure, piezoelectricity and temperature stability of $(1-x)$[$0.95(K_{0.5}Na_{0.5})NbO_3$–$0.05(Bi_{0.5}Na_{0.5})ZrO_3$]–$xCaTiO_3$–0.2%$MnO_2$ ceramics were studied. It was found that the orthorhombic-tetragonal phase transition temperature can be gradually decreased by increasing $CaTiO_3$ content. Particularly, the improved strain temperature stability (strain varied < 15% when measurement temperature reaches 110 °C) and enhanced electrical properties (d_{33} ~ 296 pC/N and strain ~ 0.14%) can be observed in the ceramics with $x = 0.02$. Therefore, shifting the T_{O-T} below room temperature is an effective way to promote temperature stability and electrical properties of KNN-based piezoelectric materials.

1 Introduction

Since $Pb(Zr,Ti)O_3$ (PZT) was reported as a ferroelectric solid solution in 1952, numerous researches have been conducted because of excellent piezoelectricity and high Curie temperature [1–4]. However, the lead oxide content in lead-based ceramics is about 60%, which can cause great harm to the environment and human health [5, 6]. With the improvement of science and technology, the awareness of environmental protection has gradually increased, and countries like the European Union, Japan and China have successively enacted laws that restrict or inhibit the use of harmful materials such as lead [6, 7]. Therefore, developing lead-free piezoelectric materials that can replace PZT-based piezoceramics has great social-economic significance.

Lead-free piezoceramics can be mainly divided into three types, including bismuth layer structure, tungsten bronze structure and perovskite structure [5]. Bismuth layer ceramics belong to strontium perovskite structure and are suitable for applications in high temperature and high frequency fields, but have a low piezoelectric performance; Tungsten bronze structure ceramics possess a high spontaneous polarization, high Curie temperature and a large optical nonlinearity, which can be used in electro optical crystals, but those ceramics are hardly sintered into dense ceramics and not easily polarized; Perovskite structure ceramics have attracted more and more attentions due to their excellent performance, which is one of the hot topics in the field of lead-free piezoelectric ceramics [5, 6]. Currently, perovskite-type lead-free piezoelectric ceramics mainly have three types: $BaTiO_3$, $Bi_{0.5}Na_{0.5}TiO_3$ and $K_{0.5}Na_{0.5}NbO_3$ [8–10]. Furthermore, Bismuth ($BiFeO_3$), one of the lead-free materials, is a multiferroic material with a distorted rhombohedral perovskite structure [11]. $BiFeO_3$ has a high remanent polarization and high Curie temperature, but the volatilization of Bi and the valence fluctuations of Fe ions in the high temperature sintering process can induce the structure loose and high leakage current [12, 13]. Lots of researches have been carried out to ameliorate the drawbacks as well improve electrical properties, including the adulteration of various ions and the addition of ABO_3-type perovskites [14–16]. $BaTiO_3$-based ceramics are the first lead-free piezoelectric ceramics to be discovered, but the low Curie temperature and high sintering temperature limit its applications. $Bi_{0.5}Na_{0.5}TiO_3$ ceramics have large remanent polarization. Although the improvements in energy storage performance, piezoelectricity and temperature stability have been realized through constructing binary and ternary compounds by doping ions or other perovskites [17–20], the existence of depolarization temperature seriously limits its development. KNN ceramics were invented

✉ Jiagang Wu
wujiagang0208@163.com; msewujg@scu.edu.cn

[1] Department of Materials Science, Sichuan University, Chengdu 610065, People's Republic of China

in 1959 [1, 10]. Currently, piezoelectric properties of KNN based ceramics can be effectively enhanced by constructing phase boundaries and optimizing experimental conditions [21–28]. Besides, By introducing local structural heterogeneity, the averaged free energy profile of a ferroelectric is possible to be further flattened and thus high piezoelectricity can be achieved [29–31]. However, the temperature stability of electrical properties is often degraded [32–36]. Previously, it was thought that the addition of $CaTiO_3$ can shift the T_{O-T} of KNN-based ceramics, and then the stability of electrical properties can be improved [37]. Unfortunately, the stability enhancement is achieved at the expense of piezoelectricity [37, 38]. Therefore, how to achieve the balanced development of piezoelectric properties and temperature stability of the ceramics is a critical consideration for us. Thus, we expect to obtain the $(1-x)[0.95(K_{0.5}Na_{0.5})NbO_3–0.05(Bi_{0.5}Na_{0.5})ZrO_3]–xCaTiO_3–0.2\%MnO_2$ ceramics with good piezoelectricity and large usage temperature range by adding $CaTiO_3$. Through the composition design, we realize the enhancement of both temperature stability and piezoelectric properties by modifying the CT contents. In addition, the underlying physical mechanisms have been illuminated.

2 Experimental process

The $(1-x)[0.95(K_{0.5}Na_{0.5})NbO_3–0.05(Bi_{0.5}Na_{0.5})ZrO_3]–xCaTiO_3–0.2\%MnO_2$ [$(1-x)$(KNN–BNZ)–xCT–MnO_2] ceramics were prepared by the convention solid-state method using K_2CO_3, Na_2CO_3, Nb_2O_5, Bi_2O_3, ZrO_2, $CaCO_3$, TiO_2 and MnO_2 as raw materials. An excess 0.2 wt% MnO_2 was added as a sintering aid to improve densification of the ceramics during the sintering process. These raw materials were weighed and ball milled with ethanol for 24 h. Then, the evenly mixed pastes were dried using a heating lamp and calcined at 850 °C for 6 h. After that, these powders were mixed with 8% PVA binder and pressed into small disks with 10 mm in diameter. After removing the binder by heating the pellets at 850 °C for 2 h, the disks were sintered at 1080–1120 °C for 3 h. Subsequently, the both sides of the sintered ceramics were covered with silver and the samples were fired at 600 °C for 10 min for measuring their electrical properties. Finally, all the specimens were polarized at room temperature in the silicon oil bath under a *dc* field of 3 kV/mm for 20 min.

The phase structure of the ceramics was tested by X-ray diffraction (Bruker D8 Advanced XRD, Bruker AXS Inc., Madison, WI, CuKa). The sintered sample was triturated into powders, and a high-resolution X-ray diffraction (X' Pert Pro MPD (DY 120 PANalytical, Netherlands)) was used to collect the XRD data of the powders for the Rietveld refinement, and then the Maud software was used for data fitting. The surface microstructure of the ceramics was characterized by a scanning electron microscope (JSM-7500, Japan). The temperature dependence of ε_r and tanδ were measured by LCR analyzer (HP 4980, Agilent, U.S.A.). A TF-2000 was used to measure the *P–E* hysteresis loops, electric field-induced strain and unipolar strain of the samples at 10 Hz. A quasi-static d_{33} meter (ZJ-3 A, China) and an impedance analyzer (HP 4194 A) were used to test the d_{33} and k_P, respectively.

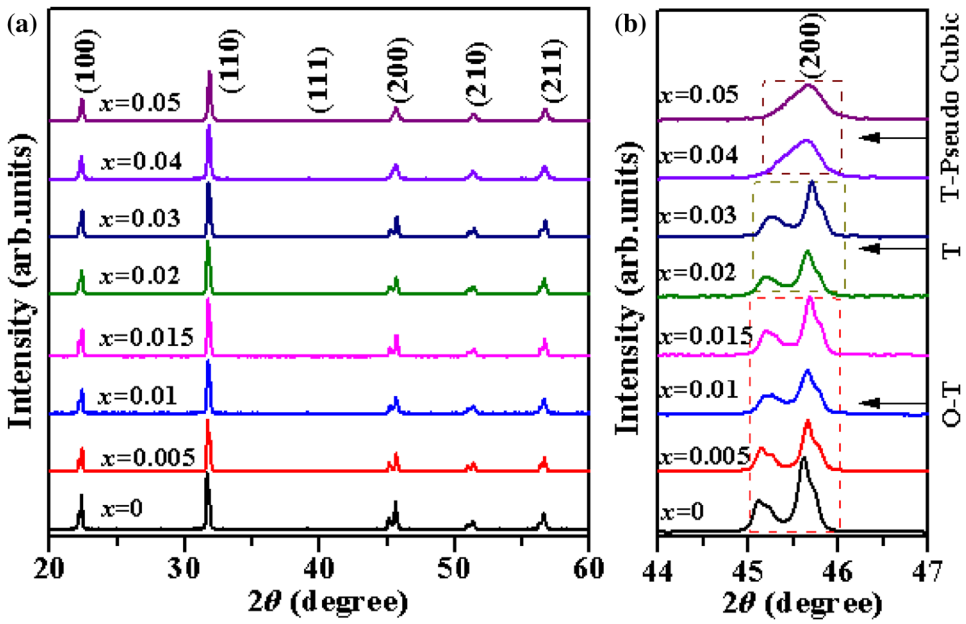

Fig. 1 **a** XRD patterns and **b** expanded XRD patterns of $(1-x)$(KNN–BNZ)–xCT–MnO_2 ceramics

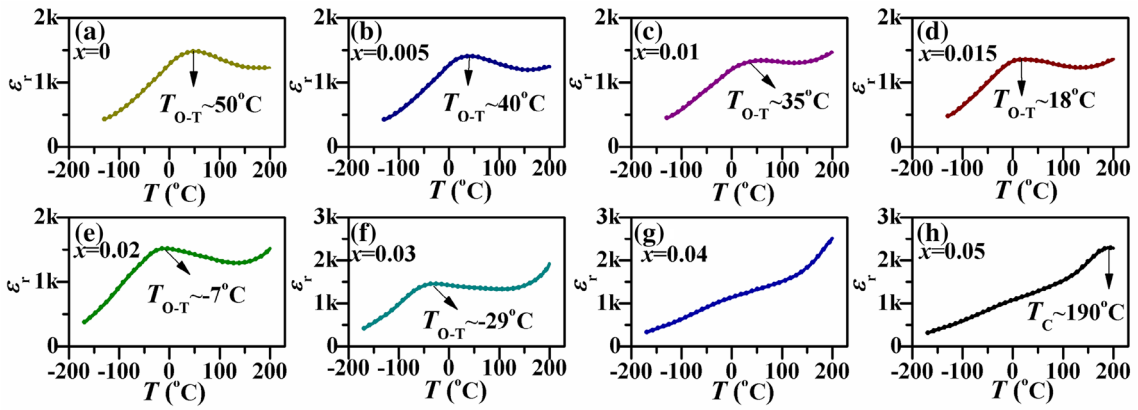

Fig. 2 ε_r of $(1-x)$(KNN–BNZ)–xCT–MnO_2 ceramics with ~ − 150 °C − 200 °C, measured at f = 100 kHz

3 Results and discussion

Figure 1a shows the XRD patterns of the ceramics, measured at room temperature and 2θ = 20°–60°. As shown in Fig. 1a, a pure perovskite structure is shown and no secondary phase can be observed in the all ceramics, indicating that BNZ, $CaTiO_3$ and MnO_2 have completely entered into the KNN matrix and formed a stable solid solution. To characterize the phase structure of all the ceramics clearly, we conduct the expended XRD patterns in the 2θ range of 44°–47°, as shown in Fig. 1b. We can see from Fig. 1b that there are two separated peaks at 2θ = 45°–46° when x = 0–0.03. The diffraction peak of high angle is clearly stronger than that of low angle, imaging the existence of tetragonal phase [39].

For further analyzing the phase evolution of the ceramics, we measured the temperature dependence of dielectric constant of all the samples, as shown in Fig. 2. The T_{O-T} of the ceramics gradually decreases from 50 °C to − 29 °C as the CT content increases, indicating that the doping of Ca^{2+} ions can significantly decrease the T_{O-T} of the ceramics far below the room temperature. So the ceramics with x = 0.02 (T_{O-T} ~ − 7 °C) can be considered as a pure T phase at room temperature. To further investigate the phase structure of the ceramics, the XRD pattern of the ceramic with x = 0.02 in powder form was measured. Figure 3a, b show the Rietveld refinement and the enlarged Rietveld refinement, respectively. Table 1 lists the detailed refinement results. The original XRD data well matched the fitting data, and a low R_w (4.84%) as well a low *Sig* (1.56) value can be observed in the fitting process, illustrating that we chose the decent phase structure mode for the ceramic (x = 0.02). Besides, the XRD results of the Rietveld refinement also confirm the existence of T phase with x = 0.02. The ceramics with x = 0.04–0.05 should be T-pseudo cubic coexistence phase, according to the XRD patterns (Fig. 1), d_{33} curves (Fig. 6) and *P*–*E* loops (Fig. 7). However, the T-pseudo phase boundary is restrained with the further increase of CT contents (x = 0.04–0.05), and becoming a diffused peak because of the decreased grain size, as shown in Figs. 2g, h and 4a [40]. In addition, the phase diagram of the $(1-x)$(KNN–BNZ)–xCT–MnO_2 ceramics can be established according to the temperature dependence of ε_r in Figs. 2 and 4a, as shown in Fig. 4b. It can be seen that T_{O-T} and T_C drop with increasing CT contents. Finally, we can give the phase structure of the ceramics by the XRD patterns, the $\varepsilon_r - T$ curves and the Rietveld

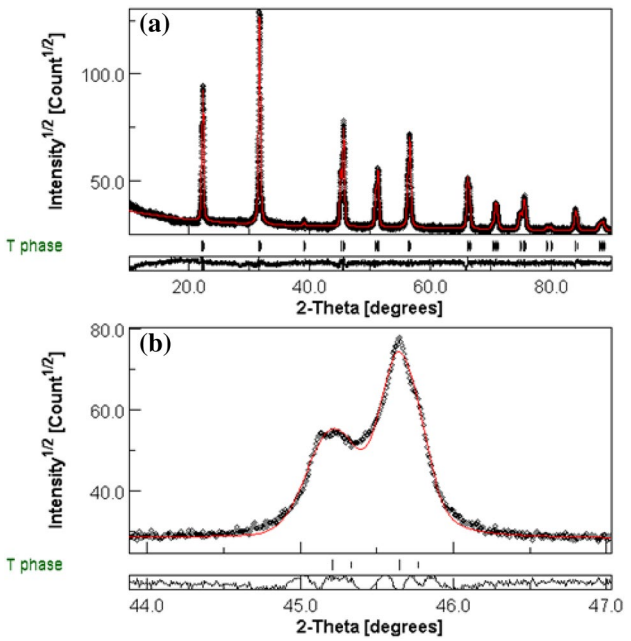

Fig. 3 **a** Rietveld refinement of XRD results with x = 0.02, **b** Enlarged Rietveld refinement of XRD patterns with x = 0.02

Table 1 Rietveld refinement of XRD results with $x = 0.02$

x (phase)	Cell parameters				Content (%)	Rw (%)	Sig
	a (Å)	b (Å)	c (Å)	α(=γ = β) (°)			
0.02 (T)	3.9715	3.9715	4.0080	90	100 (*P4mm*)	4.84	1.56

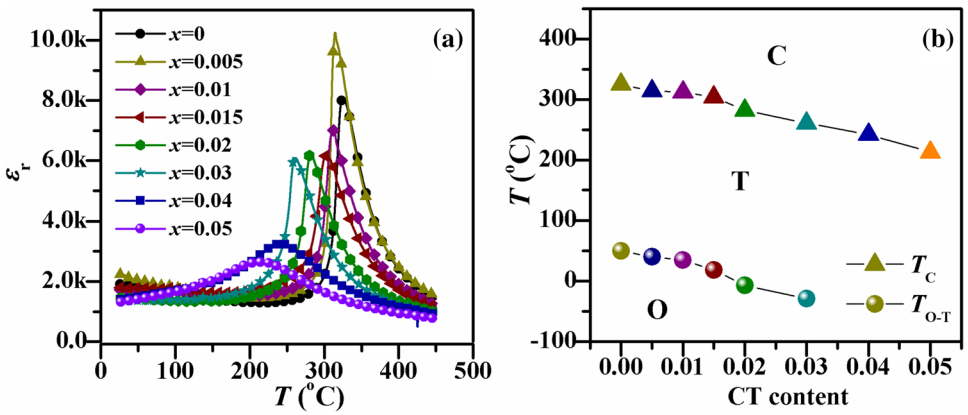

Fig. 4 **a** ε_r of $(1 - x)$(KNN–BNZ)–xCT–MnO_2 ceramics from room temperature to 450 °C, measured at $f = 100$ kHz, **b** phase diagram

refinement: O–T for $0 \leq x \leq 0.015$, T for $x = 0.02$–0.03 and T-pseudo cubic for $x = 0.04$–0.05.

Figure 5 shows the SEM micrographs procured from the surface of the sintered samples. We can see that most of grains are rectangular. Besides, it can be found that the addition of CT inhibits the growth of the grains in the ceramics. Furthermore, it is filled with small ungrown grains in the ceramics with $x = 0.04$, indicating that the excessive doping of CT contents will enrich at the grain boundary and impede the transmission of particles during the sintering process, hindering the growth of grains and forming small grains [24]. In addition, the refinement of grain in certain degree will inhibit the reversal of domain structure, thus reducing the piezoelectricity of ceramics.

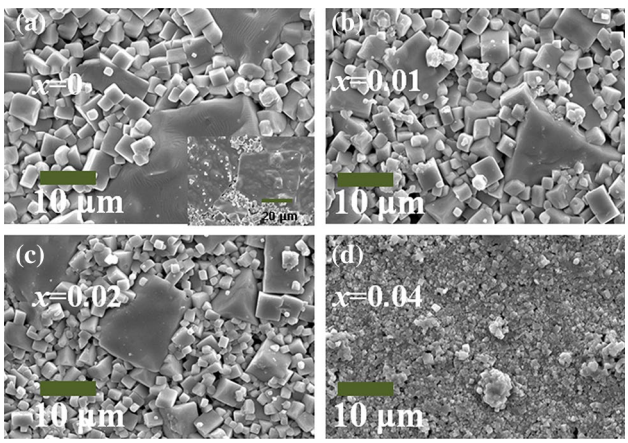

Fig. 5 SEM images of $(1 - x)$(KNN–BNZ)–xCT–MnO_2 ceramics with **a** $x = 0$, **b** $x = 0.01$, **c** $x = 0.02$, **d** $x = 0.04$

Figure 6a and b show the piezoelectric constant (d_{33}), electromechanical coupling factor (k_P), dielectric constant (ε_r) and dielectric loss (tan δ) of the ceramics as a function of CT contents, respectively. Previous researches have shown that piezoceramics can obtain large piezoelectric properties at the boundary of multiphase coexistence, owing to its easy domain switching

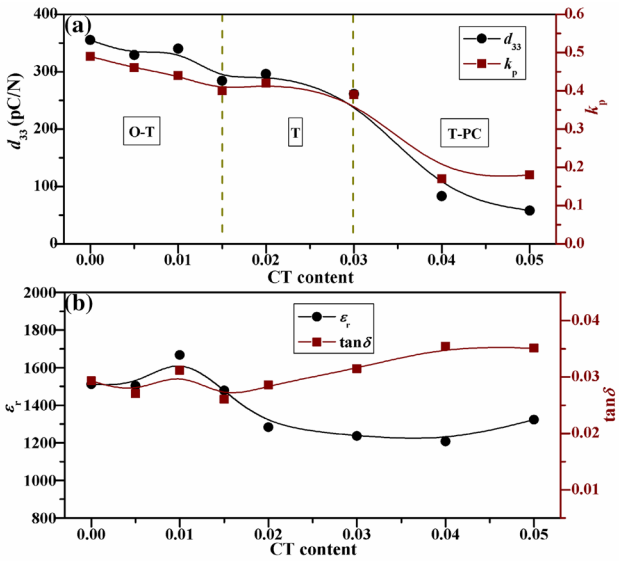

Fig. 6 **a** d_{33} and k_p of $(1 - x)$(KNN–BNZ)–xCT–MnO_2 ceramics as a function of CT contents, **b** ε_r and tan δ of $(1 - x)$(KNN–BNZ) – xCT – MnO_2 ceramics as a function of CT contents, measured at room temperature and $f = 100$ kHz

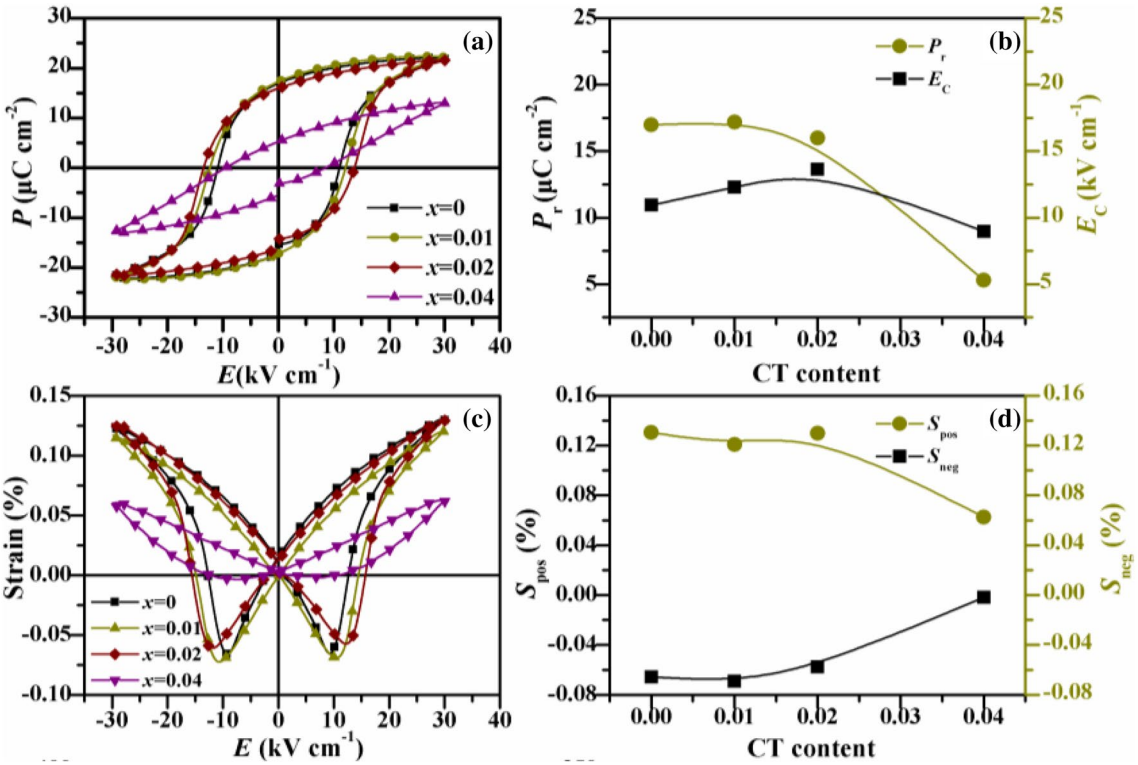

Fig. 7 **a, b** *P–E* loops of $(1-x)$(KNN–BNZ)–xCT–MnO_2 ceramics as a function of CT content, measured at room temperature and $f = 10$ Hz, **c, d** Electric field-induced strain curves

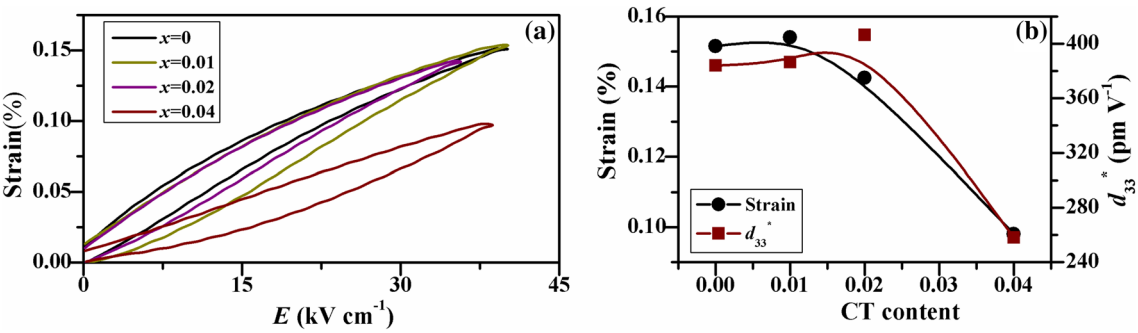

Fig. 8 **a** Unipolar strain curves of $(1-x)$(KNN–BNZ)–xCT–MnO_2 ceramics as a function of CT content, measured at room temperature and $f = 10$ Hz; **b** Unipolar strain (S_{uni}) and d_{33}* of $(1-x)$(KNN–BNZ)–xCT–MnO_2 ceramics varying with CT content

and easy polarization [22, 23]. Therefore, from Fig. 6a, we can see that the ceramics with O–T phase boundary ($x = 0$–0.01) have a relatively larger piezoelectric properties of $d_{33} = 329$–355 pC/N and $k_P = 0.44$–0.49. In contrast, the ceramics with $x \geq 0.04$ possess an inferior d_{33} due to the formation of the pseudo cubic phase. Previously, a low d_{33} of ~ 210 pC/N can be found in the KNN-based ceramics by introducing CT, due to the involvement of T phase [37]. However, a higher d_{33} of 261–296 pC/N can be observed in this work, which is attributed to composition modification. As shown in Fig. 6b, the dielectric constant increases firstly and then drops down quickly. And the dielectric loss slightly fluctuates with the variation of CT contents.

Figure 7a shows the composition dependence of *P–E* loops of the ceramics. We can see that all the ceramics have typical *P–E* loops. Moreover, the remnant polarization (P_r) and the coercive field (E_C) as a function of CT contents are

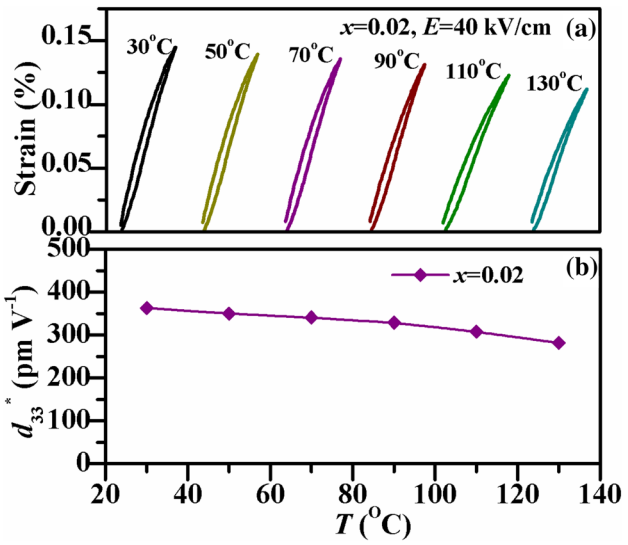

Fig. 9 **a** Temperature dependent unipolar strain of $(1-x)$(KNN–BNZ)–xCT–MnO_2 ceramics measured at room temperature and $f=10$ Hz, **b** Temperature dependence of normalized strain ($d_{33}^* = S_{max}/E_{max}$) for this work ($x=0.02$)

shown in Fig. 7b. P_r and E_C exhibit a similar trend because of the phase evolution of the samples. Besides, P_r and E_C show a downward trend after the first rise, with $x=0.01$, $x=0.02$ highest, respectively. Figure 7c gives the electric field-induced strain behavior of the ceramics. We can see that all the samples possess symmetry typical butterfly shape strain curves. As shown in Fig. 7d, the positive strain decreases gradually while the negative strain increases as the CT rises, indicating that the $\triangle S$ ($\triangle S = |S_{pos} - S_{neg}|$) descends with rising CT content. Figure 8a shows the unipolar strain curves of the ceramics. In order to clearly identify the composition dependence of unipolar strain, we portrayed the max unipolar strain and the converse piezoelectric constant of the ceramics, as shown in Fig. 8b. It can be seen that the S_{uni} and the d_{33}^* almost show a similar trend.

The temperature stability of the piezoelectricity of the ceramics is vital for the practical applications [6, 35]. Figure 9a shows the temperature stability of the unipolar strain with $x=0.02$. To clearly characterize the temperature dependence strain of the ceramics, we give the curve of normalized strain changing with temperature for this work, as shown in Fig. 9b. It is observed that normalized strain decreases linearly when the temperature increases from room temperature to 130 °C. Generally, the piezoelectricity is attributed to intrinsic and extrinsic contributions; the former is affected by lattice deformations, and the latter is influenced by domain wall motions, which is sensitive to external conditions (e.g. electric field, measurement temperature) [41, 42]. Normally, normalized strain reflects both components. Therefore, the declined normalized strain may be related to the electric field-induced phase transition and the external ambient temperature. Furthermore, strain changes in < 10% within temperature range of 30–80 °C for this work, indicating that the ceramics possess a relatively good temperature stability.

4 Conclusion

We have obtained a kind of KNN-based lead-free ceramics possessing a relatively large piezoelectricity and good temperature stability. T_{O-T} of the ceramics decreases from 50 °C to − 29 °C within the range of $0 \le x \le 0.03$, resulting in the T_{O-T} far below room temperature, and at the same time, obtaining a relatively high piezoelectricity ($d_{33}=261$–355 pC/N) and good temperature stability (e.g., unipolar strain varied less than 15% at $T=30$–110 °C). We believe that our research can promote the development of KNN-based lead free ceramics.

Acknowledgements Authors gratefully acknowledge the supports of the National Science Foundation of China (NSFC No. 51722208 and 51332003). We thank Hui Wang for measuring the SEM patterns.

References

1. G.H. Haertling, Ferroelectric ceramics: history and technology. J. Am. Ceram. Soc. **82**(4), 797–818 (1999)
2. G. Busch, Early history of ferroelectricity. Ferroelectrics **74**(1), 267–284 (1987)
3. J. Fousek, Ferroelectricity: remarks on historical aspects and present trends. Ferroelectrics **113**(11), 3–20 (1991)
4. K. Wang, B. Malic, J.G. Wu, Shifting the phase boundary: potassium sodium niobate derivates. MRS Bull. **43**(8), 607–611 (2018)
5. E. Cross, Materials science-lead-free at last. Nature **432**(7013), 24–25 (2004)
6. J.G. Wu, D.Q. Xiao, J.G. Zhu, Potassium-sodium niobate lead-free piezoelectric ceramics: recent advances and perspectives. Chem. Rev. **115**(7), 2559–2595 (2015)
7. J. Koruza, A.J. Bell, T. Fromling et al., Requirements for the transfer of lead-free piezoceramics into application. J. Materiomics **4**(1), 13–26 (2018)
8. T.M. Amaral, E. Antonelli, D.A. Ochoa et al., Microstructural features and functional properties of bilayered $BaTiO_3/BaTi_{1-x}Zr_xO_3$ ceramics. J. Am. Ceram. Soc. **98**(4), 1169–1174 (2015)
9. H. Nagata, T. Takenaka, Additive effects on electrical properties of $(Bi_{1/2}Na_{1/2})TiO_3$ ferroelectric ceramics. J. Eur. Ceram. Soc. **21**(10), 1299–1302 (2001)
10. L. Egerton, D.M. Dillon, Piezoelectric and dielectric properties of ceramics in the system potassium-sodium niobate. J. Am. Ceram. Soc. **42**(9), 438–442 (1959)
11. N.S. Zhao, H.Q. Fan, X.H. Ren et al., Dielectric, conductivity and piezoelectric properties in $(0.67-x)BiFeO_3$-$0.33BaTiO_3$-$xSrZrO_3$ ceramics. Ceram. Int. **44**(15), 18821–18827 (2018)
12. S. Murakami, D.W. Wang, A. Mostaed et al., High strain (0.4%) $Bi(Mg_{2/3}Nb_{1/3})O_3$-$BaTiO_3$-$BiFeO_3$ lead-free piezoelectric ceramics and multilayers. J. Am. Ceram. Soc. **101**(12), 5428–5442 (2018)

13. D.W. Wang, A. Khesro, S. Murakami et al., Temperature dependent, large electromechanical strain in Nd-doped $BiFeO_3$-$BaTiO_3$ lead-free ceramics. J. Eur. Ceram. Soc. **37**(4), 1857–1860 (2017)
14. D.W. Wang, Z.M. Fan, D. Zhou et al., Bismuth ferrite-based lead-free ceramics and multilayers with high recoverable energy density. J. Mater. Chem. A **6**(9), 4133–4144 (2018)
15. D.W. Wang, Z.M. Fan, W.B. Li et al., High energy storage density and large strain in $Bi(Zn_{2/3}Nb_{1/3})O_3$-doped $BiFeO_3$-$BaTiO_3$ ceramics. ACS Appl. Energy Mater. **1**(8), 4403–4412 (2018)
16. S. Murakami, N.T.A.F. Ahmed, D.W. Wang et al., Optimising dopants and properties in BiMeO3 (Me = Al, Ga, Sc, Y, $Mg_{2/3}Nb_{1/3}$, $Zn_{2/3}Nb_{1/3}$, $Zn_{1/2}Ti_{1/2}$) lead-free $BaTiO_3$-$BiFeO_3$ based ceramics for actuator applications. J. Eur. Ceram. Soc. **38**(12), 4220–4231 (2018)
17. B. Hu, A.Q. Fan, L. Ning et al., Enhanced energy-storage performance and dielectric teemperature stability of (1-*x*)$(0.65Bi_{0.5}Na_{0.5}TiO_3$-$0.35Bi_{0.1}Sr_{0.85}TiO_3)$-*x*$KNbO_3$ ceramics. Ceram. Int. **44**(9), 10968–10974 (2018)
18. G.Z. Dong, H.Q. Fan, J. Shi et al., Composition-and temperature-dependent large strain in (1-*x*)$(0.8Bi_{0.5}Na_{0.5}TiO_3$-$0.2Bi_{0.5}K_{0.5}TiO_3)$-*x*$NaNbO_3$ ceramics. J. Am. Ceram. Soc. **98**(4), 1150–1155 (2015)
19. N.S. Zhao, H.Q. Fan, X.H. Ren et al., A Novel $((Bi_{0.5}Na_{0.5})0.94Ba_{0.06})_{1-x}(K_{0.5}Nd_{0.5})_xTiO_3$ lead-free relaxor ferroelectric ceramic with large electrostrains at wide temperature ranges. Ceram. Int. **44**(1), 571–579 (2018)
20. N.S. Zhao, H.Q. Fan, J.W. Ma et al., Large strain of temperature insensitive in(1-*x*)$(0.94Bi_{0.5}Na_{0.5}TiO_3$-$0.06BaTiO_3)$-*x*$Sr_{0.7}La_{0.2}TiO_3$ lead-free ceramics. Ceram. Int. **44**(10), 11331–11339 (2018)
21. T. Zheng, J.G. Wu, D.Q. Xiao et al., Recent development in lead-free perovskite piezoelectric bulk materials. Prog. Mater. Sci. **98**, 552–624 (2018)
22. L. Fu, L. Lin, Y.R. Luo et al., Development of the electrical properties of KNN-based lead-free piezoceramics based on the phase boundary building and ternary composition designing. Mater. Res. Bull. **94**, 506–512 (2017)
23. X.P. Wang, J.G. Wu, D.Q. Xiao et al., Giant piezoelectricity in potassium-sodium niobate lead-free ceramics. J. Am. Chem. Soc. **136**(7), 2905–2910 (2014)
24. X.P. Wang, J.G. Wu, X.J. Cheng et al., Compositional dependence of phase structure and electrical properties in $(K_{0.5}Na_{0.5})_{0.75}Bi_{0.01}(Nb_{1-x}Zr_x)O_3$ lead-free ceramics. Ceram. Int. **39**, 8021–8024 (2013)
25. K. Xu, J. Li, X. Lv et al., Superior piezoelectric properties in potassium-sodium niobate lead-free ceramics. Adv. Mater. **28**, 8519–8523 (2016)
26. Z. Wang, D.Q. Xiao, J.G. Wu et al., New lead-free (1-*x*)$(K_{0.5}Na_{0.5})NbO_3$-*x*$(Bi_{0.5}Na_{0.5})ZrO_3$ ceramics with high piezoelectricity. J. Am. Ceram. Soc. **97**(3), 688–690 (2014)
27. P. Tan, H. Tian, C.P. Hu et al., Field-driven electro-optic dynamics of polar nanoregions in nanodisordrerd $KTa_{1-x}Nb_xO_3$ crustal. Appl. Phys. Lett. **111**(1), 012903 (2017)
28. P. Tan, H. Tian, C.P. Hu et al., Temperature field driven polar nanoregions in $KTa_{1-x}Nb_xO_3$. Appl. Phys. Lett. **109**(25), 252904 (2016)
29. F. Li, D.B. Lin, Z.B. Chen et al., Ultrahigh piezoelectricity in ferroelectric ceramics by design. Nat. Mater. **17**(4), 349–354 (2018)
30. F. Li, S.J. Zhang, T.N. Yang et al., The origin of ultrahigh piezoelectricity in relaxor-ferroelectric solid solution crystals. Nat. Commun. **7**, 13807 (2016)
31. F. Li, S.J. Zhang, D. Damjanovic et al., Local structural heterogeneity and electromechanical responses of ferroelectrics: learning from relaxor ferroelectrics. Adv. Funct. Mater. **28**(37), 1801504 (2018)
32. F.Z. Yao, Q. Yu, K. Wang et al., Ferroelectric domain morphology and temperature-dependent piezoelectricity of (K,Na,Li)(Nb,Ta,Sb)O_3 lead-free piezoceramics. RSC. Adv. **4**, 20062–20068 (2014)
33. T. Z, W.J. Wu, J.G. Wu et al., Balanced development of piezoelectricity, curie temperature, and temperature stability in potassium-sodium niobate lead-free ceramics. J. Mater. Chem. C. **4**, 9779–9787 (2016)
34. R. Wang, K. Wang, F.Z. Yao et al., Temperature stability of lead-free niobate piezoceramics with engineered morphotropic phase boundary. J. Am. Ceram. Soc. **98**(7), 2177–2182 (2015)
35. K. Wang, F.Z. Yao, W. Jo et al., Temperature-insensitive (K,Na)NbO_3-based lead-free piezoactuator ceramics. Adv. Funct. Mater. **23**(33), 4079–4086 (2013)
36. F.Z. Yao, K. Wang, W. Jo et al., Diffused phase transition boosts thermal stability of high-performance lead-free piezoelectrics. Adv. Funct. Mater. **26**, 1217–1224 (2016)
37. S.J. Zhang, R. Xia, T.R. Shrout, $K_{0.5}Na_{0.5}NbO_3$ based lead-free piezoelectrics with broad temperature usage range. Appl. Phys. Lett. **91**, 132913 (2007)
38. J.G. Wu, D.Q. Xiao, Y.Y. Wang et al., $CaTiO_3$-modified $(K_{0.5}Na_{0.5})(Nb_{0.96}Sb_{0.04})O_3$ lead-free piezoelectric ceramics. J. Am. Ceram. Soc. **91**(10), 3402–3404 (2008)
39. X. Lv, J.G. Wu, S. Yang et al., Identification of phase boundaries and electrical properties in ternary potassium-sodium niobate based ceramics. ACS Appl. Mater. Interfaces **8**, 18943–18953 (2016)
40. X.J. Cheng, J.G. Wu, T. Zheng et al., Rhombohedral-tetragonal phase coexistence and piezoelectric properties based on potassium-sodium niobate ternary system. J. Alloys Compd. **610**, 86–91 (2014)
41. D.W. Wang, F. Hussain, A. Khesro et al., Composition and temperature dependence of structure and piezoelectricity in (1-*x*)$(K_{1-y}Na_y)NbO_3$-*x*$(Bi_{1/2}Na_{1/2})ZrO_3$ lead-free ceramics. J. Am. Ceram. Soc. **100**(2), 627–637 (2017)
42. J.S. Zhou, K. Wang, F.Z. Yao et al., Multi-scale thermal stability of niobate-based lead-free piezoceramics with large piezoelectricity. J. Mater. Chem. C **3**(34), 8780–8787 (2015)